



# Investigating the wind-wave interaction on mean wind and turbulence structure using COAWST with WRF-LES

Sima Hamzeloo<sup>a</sup>, Xiaoli Guo Larsén<sup>a</sup>, Alfredo Peña<sup>a</sup>, Jana Fischereit<sup>a</sup>, and Oscar García-Santiago<sup>a</sup>

<sup>a</sup>Technical University of Denmark, Frederiksborgvej 399, Roskilde 4000, Denmark

**Correspondence:** Sima Hamzeloo (siham@dtu.dk)

**Abstract.** We investigate wind-wave interactions within the marine atmospheric boundary layer during a storm event over the North Sea, using a multiscale coupled modeling framework. Large eddy simulations run within the Weather Research and Forecasting model have been coupled with the Simulating WAves Nearshore model through the Coupled Ocean-Atmosphere-Wave-Sediment Transport system. The simulation consists of six nested domains, three outer mesoscale domains with horizontal grid spacings (9.9, 3.3, and 1.1 km), and three innermost large eddy simulation domains with coarse and fine horizontal grid spacings. Wind and wave outputs from both the finest mesoscale domain and the coarsest LES domain are evaluated against metocean and lidar measurements collected during the storm. The results show that the coarsest LES domain represents wind speeds up to 150 m height more accurately than the mesoscale output but due to excessive simulated vertical wind shear. Above this height, the mesoscale and LES outputs become much closer, and both tend to overestimate the wind speed. The wind direction is well captured across both domains. The significant wave height, peak wave period, and mean wave direction simulated by SWAN show better agreement with observations when forced by the LES output than the mesoscale output. Additionally, the coupled simulations exhibit stronger turbulence fluxes than the uncoupled simulations, which is clearly observed in the vertical profiles of velocity variances and covariances. These findings demonstrate the benefits of high-resolution coupled modeling for capturing offshore boundary layer dynamics and improving wind and wave predictions under severe weather conditions.

## 15 1 Introduction

Accurate understanding of the structure of the marine atmospheric boundary layer (MABL), including mean wind profiles and turbulence characteristics, has become increasingly important in recent decades due to the global expansion of offshore wind energy, and it is listed as one of the grand challenges for wind energy research (Shaw et al., 2022). The physical processes in the MABL can be more complex than those over land due to additional interactions at the air-sea interface, which span 20 multiple temporal and spatial scales. These interactions, particularly involving ocean waves, can modify the atmospheric flow up to hub height and above (Kalvig et al., 2014; Porchetta et al., 2022; Jenkins et al., 2012; Yang et al., 2014; Fischereit et al., 2022), affecting wind resource assessments, turbine loading, and energy yield predictions. Such complexities require advanced, high-resolution modeling strategies (Shaw et al., 2022).

Atmospheric motions within the MABL are impacted by mesoscale weather systems down to turbulent eddies. Numerical 25 models are typically designed to operate at a range of scales, and as a result, studies often rely on a variety of parameteriza-



tions and configurations to bridge the gap between mesoscale and microscale dynamics, (Sullivan et al., 2008; Hamzeloo et al., 2025). Our understanding of coupled wind–wave dynamics has been limited by the difficulty of capturing at the same time both mesoscale weather variability and microscale turbulence over realistic ocean surfaces. To address this, Ning et al. (2023) evaluated the parameterizations of sea surface roughness in a multiscale simulation framework, employing the Weather Research 30 and Forecasting (WRF) model coupled with the Simulating of WAve Nearshore (SWAN) model for mesoscale processes. The output of the wave-influenced roughness parameterization was fed into the Parallelized Large-eddy Simulation Model (PALM) rather than being directly coupled to the wave model. Their results showed that, although the framework reproduced mean wind and turbulence characteristics under realistic offshore conditions, it exhibited minimal sensitivity to different roughness parameterizations. Additionally, the use of a one-way meso-to-micro coupling meant that full two-way interactions between 35 scales were not resolved. They suggested that future work should explore two-way coupling strategies and more advanced wind–wave parameterizations.

These limitations underscore the need for a multiscale modeling framework that integrates mesoscale and microscale processes. Such approaches allow for nesting high-resolution LES domains within mesoscale simulations, enabling the representation of both synoptic-scale variability and fine-scale turbulence. In these frameworks, mesoscale atmospheric conditions 40 provide realistic time-varying boundary forcing for the embedded LES, allowing us to resolve small-scale turbulence and wave-induced feedback that would otherwise be missed in coarser models. Multiscale simulations driven by time-varying atmospheric conditions are able to represent meteorological processes on land with large-scale variations in wind and temperature, as well as the associated turbulent flow structures across scales (Muñoz-Esparza et al., 2017). In the present work, the meso-to-micro coupling is extended to offshore conditions, where both the mesoscale and the LES domains are explicitly 45 coupled with a wave model to represent wind–wave interactions in the MABL, which has not been fully addressed in earlier multiscale studies.

The Coupled Ocean-Atmosphere-Wave-Sediment Transport (COAWST) modeling system (Warner et al., 2010) is a well-established tool for simulating air-sea interactions. The COAWST framework integrates several modeling components comprising the model coupling toolkit to exchange data fields between an ocean model (ROMS), an atmospheric model WRF, 50 a wave model SWAN, and a sediment transport model. Numerous studies have utilized COAWST to investigate a variety of air–sea interaction processes (Cambazoglu et al., 2024; Jiang et al., 2025). To our knowledge, to date, all coupling between the components of the WRF and SWAN models within the COAWST framework has been performed at mesoscale resolutions. For example, in the field of offshore wind energy, studies have examined interactions between wind, waves, and wakes 55 (Larsén et al., 2024; Fischereit et al., 2022), while others have focused on hurricanes and extreme tropical cyclones (Chen et al., 2024; Alimohammadi et al., 2020; Olabarrieta et al., 2012). Larsén et al. (2019) used COAWST to compare roughness-length parameterizations with direct stress coupling for wave–atmosphere interactions. They found that stress-based coupling better captured the observed wind field in synthetic aperture radar from an offshore wind farm.

To the best of our knowledge, this study is the first to enable a multiscale online two-way air-sea coupled system by integrating LES in the WRF model with the SWAN wave model within the COAWST framework. This approach allows for the 60 investigation of high-resolution interactions during a selected storm event, enhancing our understanding of coupled wind-wave



dynamics. We focus on an extreme wind and wave event, following our previous study (Hamzeloo et al., 2025), in which we investigated the effects of waves on mean wind speed, direction, turbulence fluxes and spectral characteristics using a one-way offline coupling between WRF-LES and the MIKE3 Wave FM model (M3W) (DHI, 2024). That study was conducted under idealized conditions. Here, we build on that work by performing a fully coupled weather-driven multiscale simulation using 65 WRF and SWAN, allowing for a more realistic assessment of wave effects on MABL dynamics.

This paper is structured as follows: Section 2 describes the methodology, including a description of the measurement data, the model setup for both wind and wave components, and the coupling strategy. Section 3 presents the simulation results. Sections 4 and 5 provide discussion and conclusions, respectively.

## 2 Methodology

### 70 2.1 Measurements and the selected case

We use wind and wave measurements from the Reducing the Uncertainty of Nearshore Experiment (RUNE) project to evaluate wind and wave simulations. RUNE was a collaborative research project that conducted a coastal offshore measurement campaign from November 2, 2015, to March 1, 2016, near the west coast of Jutland, Denmark. The experiment and data collected during RUNE are described in detail by Floors et al. (2016) and Bolaños and Rørbæk (2016).

75 During the campaign, wind and wave measurements were taken approximately 7 km offshore. Wave measurements were obtained using a directional Triaxy wave buoy equipped with a downward-looking acoustic Doppler current profiler. This buoy was deployed at the beginning of the campaign at a water depth of 16.5 m. The hourly integrated wave parameters—including significant wave height ( $H_s$ ), maximum wave height ( $H_{max}$ ), peak wave period ( $T_p$ ), average zero-crossing period ( $T_{02}$ ), and mean wave direction (MWD) are processed from the 7 Hz sampled data. A lidar buoy, positioned less than 200 m from the 80 wave buoy, was equipped with a WindCube® v2 Doppler wind lidar to record wind data. Mean wind speed and direction are available every 10 minutes at 12 different heights above mean sea level: 40, 47, 59, 79, 97, 117, 134, 147, 172, 197, 209, and 247 m.

Figure 1 presents the time series of  $H_s$  and the wind speed at a height of 40 m, and MWD and wind direction at a height of 40 m, for a period of a week around our focus day. The wind measurements shown in the plots correspond to the lowest 85 recorded height. We observe a good wind-wave alignment from the southwest, which lasts for almost a full day on the 5th of December, marked as gray in Fig. 1. Additionally, the most intense wave event during the measurement period occurred on the same day, at 18:00 UTC, when the  $H_s$  reached 5.77 m, and the average zero-crossing period ( $T_{02}$ ) was 8.7 s. During this storm, the average wind speed ranged from  $21.3 \text{ m s}^{-1}$  at 40 m to  $26.8 \text{ m s}^{-1}$  at 247 m. We use this day to investigate the wind-wave interaction in the COAWST modeling system in LES mode. This event is selected to investigate wind-wave interactions 90 using the two-way online coupled WRF-LES–SWAN system, building on previous studies that validated the offline one-way coupling of WRF-LES with the MIKE3 Wave model (Hamzeloo et al., 2025) using RUNE measurements.

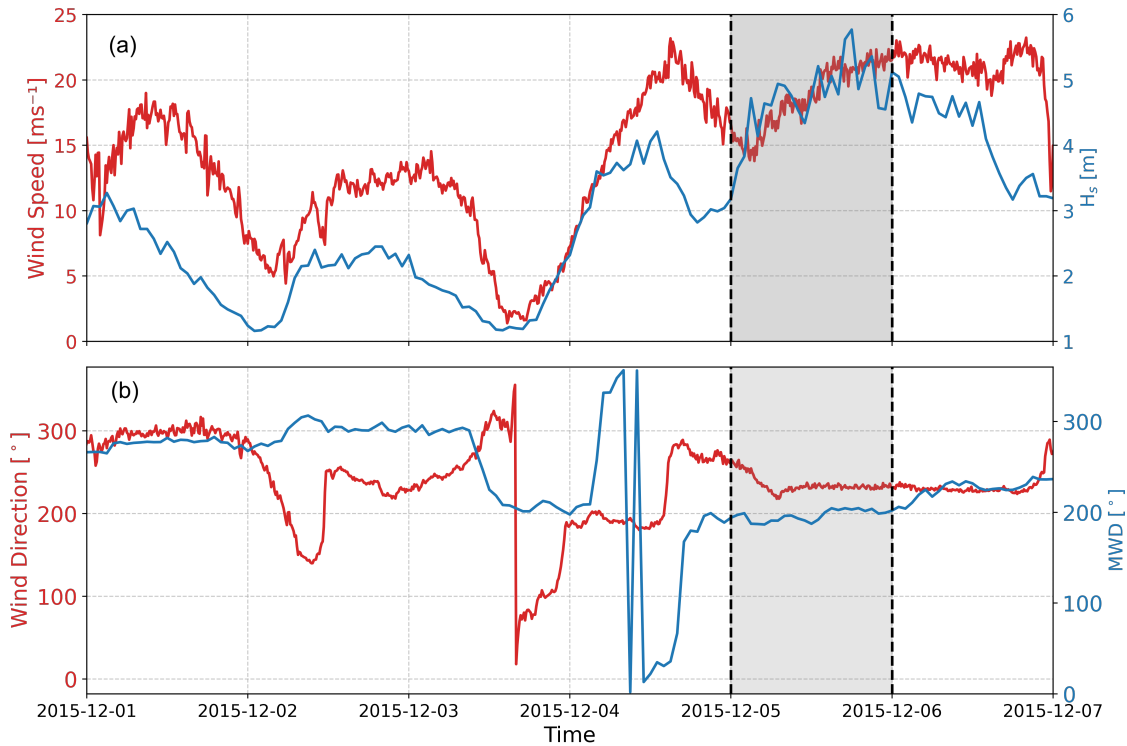


**Figure 1.** Time-series of wind speed (a) and direction (b) on the left axis and significant wave height  $H_s$  (a) and mean wave direction (MWD) (b) on the right axis, from measurements of the wave buoy and from measurements of the lidar at a 40-m height, respectively. The gray range shows the period we selected for this study.

## 2.2 Modeling system

We utilize the WRF model, version 4.5 (Skamarock et al., 2019) and SWAN model, version 41.45 (Booij et al., 1997) through the COAWST modeling system version 3.8 (Warner et al., 2010) to simulate wind-wave interactions in the North Sea for the 95 selected storm. Other components of the COAWST system are not activated in this study. The WRF and SWAN models are two-way coupled online through the wave boundary layer model (WBLM) implemented in SWAN (Du, 2017; Du et al., 2019). The WBLM accounts for the vertical variation of stresses and energy in the wave boundary layer (WBL), which is the interface between the waves and the atmospheric boundary layer above it. In this region, the wind speed profile deviates from the classical logarithmic shape due to wave-induced motions and momentum exchange. In this coupled system, the WRF horizontal velocity 100 components at the height of 10 m (longitudinal  $U$ , and meridional  $V$ , respectively) are sent to SWAN. The WBLM uses the former velocities along with local wave-induced and turbulent stress, and wave phase velocity, to calculate the vertical wind profile within the WBL by solving the kinetic energy conservation equation and calculates the equivalent roughness length ( $z_0$ )



**Table 1.** Domain configurations of the simulations.  $\Delta x$  corresponds to horizontal grid spacing,  $N_x$  and  $N_y$  to number of grid points in  $x$  and  $y$  direction and  $\Delta t$  to numerical integration time step.

Simulations	Domains	$\Delta x$ [m]	Nest Ratio	$N_x \times N_y$	$\Delta t$ [s]	PBL/SGS
WRF/	D01	9900	–	101 $\times$ 101	45	YSU
WRF-SWAN	D02	3300	3	112 $\times$ 112	15	YSU
	D03	1100	3	121 $\times$ 121	5	YSU
WRF-LES/	D04	100	11	309 $\times$ 276	0.450	Deardorff
WRF-LES-SWAN	D05	20	5	301 $\times$ 301	0.090	Deardorff
	D06	4	5	301 $\times$ 301	0.018	Deardorff

that conforms to the logarithmic wind profile, and finally transfers  $z_0$  back to the surface module of the WRF model (Fischereit et al., 2022; Du et al., 2022), resulting in more realistic wave growth and improved energy exchange at the air–sea interface.

105 We perform multiscale modeling within the COAWST system to support the coupling strategy across different spatial scales. For this, we activate a multiscale modeling setup within the COAWST system. Unlike most previous COAWST applications, which remain limited to mesoscale resolutions, our configuration extends the coupling to include LES domains. To make this framework operational, we applied two key adjustments. First, in the finer domains with 100 m grid spacing, we replaced the planetary boundary layer (PBL) scheme with LES. Second, we implemented the cell perturbation method (CPM) 110 (Muñoz-Esparza et al., 2015; Muñoz-Esparza and Kosović, 2018) in the WRF model within the COAWST framework to enable turbulence simulations.

### 2.3 Simulations

Our multiscale WRF simulations include six nested domains. The outer three domains run in mesoscale mode with horizontal 115 grid spacings of 9.9, 3.3, and 1.1 km, respectively, while the inner three domains run in LES mode. The coarsest LES domain has a grid spacing of 100 m. The grid spacing ratio between mesoscale domains is 1:3, while the ratio from the finest mesoscale to the coarsest LES domain is 1:11. Then, we nested two more LES domains with a 1:5 grid spacing ratio of 20 m and 4 m, which are run for a shorter period (10 hours). The time step ratio matches the grid spacing ratio, with a time step of 45 s for the outermost domain. All four domains consist of 61 vertical levels, with the first level located 10 m above the surface. The 120 model's top is at 5000 Pa. The SWAN model adopts the same domain configuration as presented in Fig. 2. More details on the model domain specifications can be found in Table 1.

The outermost domain is initialized and forced using ERA5 reanalysis data, updated every six hours (C3S, 2017). In addition, the Operational Sea Surface Temperature and Sea Ice Analysis (OSTIA) dataset is used to update the sea surface temperature and sea ice fields during simulations (Donlon et al., 2012). For static inputs, we utilize the default datasets provided by the WRF model, along with the CORINE Land Cover dataset (Feranec, 2016) and the ESA Climate Change Initiative (CCI) Land 125 Cover datasets at resolutions of 100 m and 300 m, respectively (Bontemps et al., 2013).

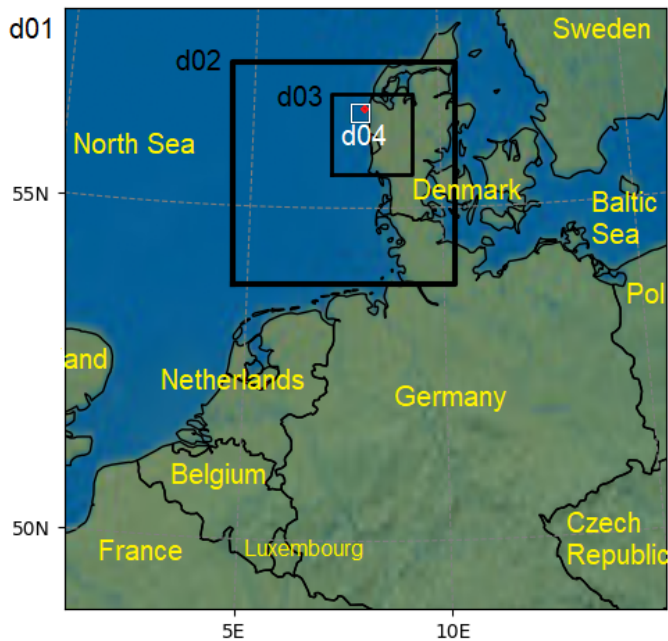


**Figure 2.** Nested domains configuration for our simulations. The red dot in the upper right of D04 is the location of RUNE measurements. D05 and D06 located within D04 are not shown.

For the physics parameterizations of the WRF model, we employ the WRF Single-Moment 6-Class (WSM 6-class) graupel scheme for microphysics (Hong et al., 2004), which includes predictive variables for water vapor, cloud water/ice, rain, snow, and graupel. For radiation processes, we utilize the Rapid Radiative Transfer Model (RRTM) (Mlawer et al., 1997) for longwave radiation and the Dudhia scheme (Dudhia, 1989) for shortwave radiation, both executed every 9 min/km, as recommended. The 130 Kain-Fritsch scheme (Kain and Fritsch, 1993) is employed for cumulus parameterization, activated every 5 min exclusively for the outermost domain. The Unified Noah land surface model (Tewari et al., 2004) is applied for land surface, while the Revised MM5 Monin-Obukhov scheme is used for the surface layer. The Yonsei University (YSU) scheme (Hong et al., 2006) is used for PBL parameterization, which was selected based on a sensitivity analysis among three other schemes: the Mellor-Yamada-Nakanishi-Niino (MYNN) (Nakanishi and Niino, 2006), Mellor-Yamada-Janjić (MYJ) (Janjić, 2002), and Quasi-Normal Scale 135 Elimination (QNSE) (Sukoriansky et al., 2005) schemes. PBL schemes are deactivated for the innermost domains as they run in LES mode with a subgrid-scale (SGS) model that uses a 1.5-order turbulence kinetic energy (TKE) closure (Deardorff, 1980). The closure prognoses the TKE, which is used to compute the local eddy diffusivity.

In multiscale simulations using the WRF model, turbulence in the LES domain may not develop fast enough because of the smooth flow from the parent mesoscale domain and the time needed for high resolution LES domain to develop turbulence. The 140 PBL scheme assumes horizontal homogeneity within each grid cell, which contrasts with the LES domain where turbulence is explicitly resolved using a SGS model that represents the Reynolds stress tensor and turbulent kinetic energy (TKE) (Muñoz-



Esparza et al., 2014). This challenge is further intensified in offshore areas, where the absence of topographical features limits the production of turbulence. To address this issue and promote a seamless transition from mesoscale boundary conditions to fully developed LES turbulence, the CPM is applied at the inflow boundaries of the LES domain. In this study, we integrate 145 the CPM into the WRF model within the COAWST framework for the first time, enabling the application of this technique in coupled ocean–atmosphere–wave simulations. The CPM method (Muñoz-Esparza et al., 2015) introduces controlled perturbations. We use three perturbation cells to develop realistic turbulent fields (Peña and Mirocha, 2024). Additionally, we conduct a simulation without activating CPM in the LES domain (D04) to assess its impact on the simulations, which is presented in 3.4.

150 We initialize the SWAN model using the output spectrum at each grid cell from a previous simulation conducted 24 hr earlier to allow for spin-up and provide consistent boundary conditions. The open boundaries of the outermost domain are set to zero. This does not impact the innermost domains due to the large domain size. We utilized 36 directional bins with a frequency exponent of 1.1. The frequency range extends from 0.03 to 10.05 Hz, resulting in a total of 61 frequency bins. The SWAN model operates with a time step of 6 min for the four outermost domains, and the time step is reduced to 4 min for 155 D05 and D06. The EMODnet Digital Terrain Model (DTM) with a grid resolution of 1/8 arc-min (approximately 230 m) is used for the bathymetry. In addition to the configurations mentioned above, the SWAN model incorporates several physical processes to accurately simulate wave dynamics. The depth-induced wave break is modeled using the parameters  $\alpha = 1.0$  and  $\gamma = 0.73$ , which control the intensity and the break threshold, respectively. Bottom friction is taken into account using the JONSWAP formulation with a friction coefficient of 0.038, representing energy dissipation due to seabed interactions. White- 160 capping dissipation, which addresses the energy loss from wave breaking in deep water, is activated using the WAM Cycle 3 formulation with drag law fitting.

Simulations for D01 to D04 are run over a 30-hr period from 18:00 UTC on December 4 to 00:00 UTC on December 6 for both coupled and uncoupled models. Simulations for D05 and D06 are run for a shorter period of 10 h with the same starting time (for both coupled and uncoupled simulations). Results and analysis focus on the entire December 5 for D01 to D04, and 165 on the first 4 hours of this day for D05 and D06, which we use for turbulence analysis. The SWAN model outputs were saved every 10 min for both D03 and D04 domains. For the WRF model, outputs were saved every 10 min for D03 and every 10 s for D04, D05, and D06.

### 3 Results

In this section, we evaluate the outputs from the WRF and SWAN models by comparing simulated wind and wave data from 170 the finest mesoscale domain (D03) and the coarsest LES domain (D04) with RUNE observations. The simulation outputs are extracted at the grid point closest to the RUNE site. After the validation, we analyze the turbulence fluxes from D04, D05, and D06. Results from D05 and D06 are not used for the validation, as they are run only for a few hours, and the main aim of simulating in this fine domain is to investigate the effect of horizontal grid spacing on turbulence fluxes.



### 3.1 Evaluation of simulated wave parameters

175 Figure 3 presents a comparison of  $H_s$ , MWD, and  $T_p$  derived from SWAN when coupled with both the mesoscale (D03) and LES (D04) domains against RUNE buoy measurements. The 10-min simulation outputs were averaged over hourly intervals to match the temporal resolution of the hourly integrated measured wave parameters. The corresponding values of the root mean square error (RMSE) for each domain, calculated relative to the observations, are summarized in Table 2. The results indicate that, while model outputs in both domains follow the observed data, the LES-driven output provides improved wave  
 180 characteristics, particularly for  $H_s$ , with an RMSE nearly half that of the mesoscale-driven domain output. The simulated  $T_p$  and MWD exhibit only minor differences between the two domains.

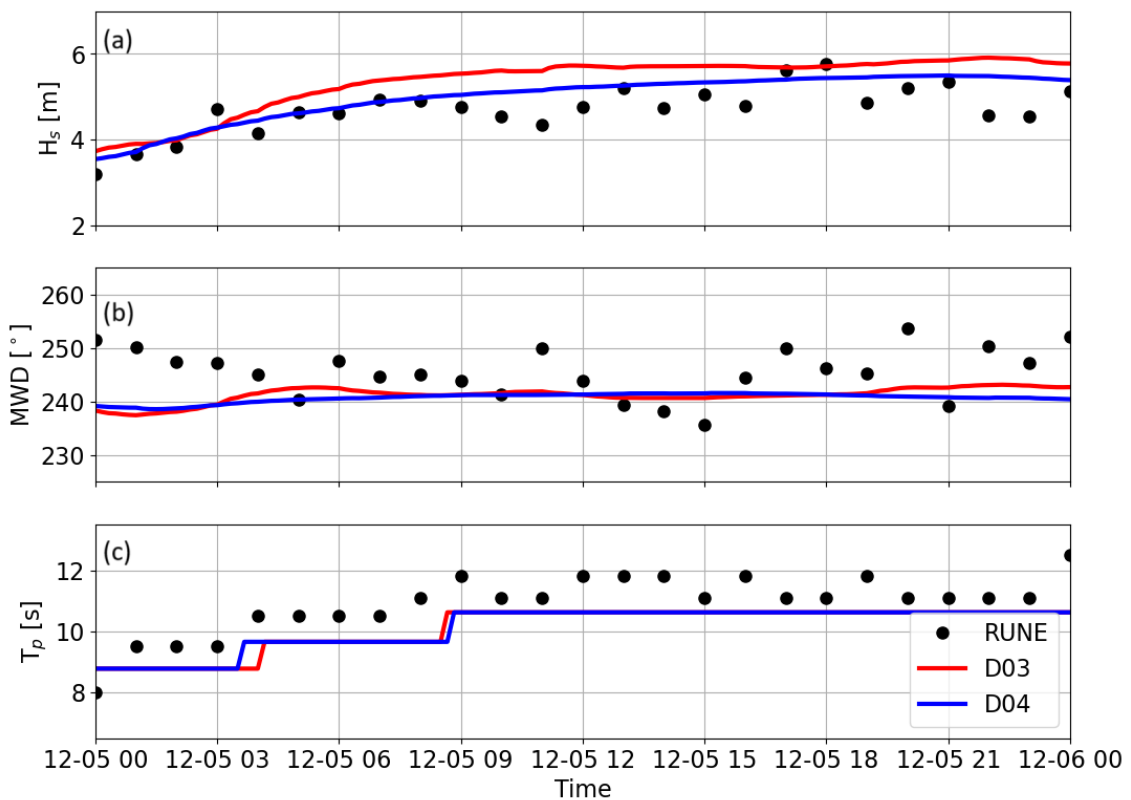


**Figure 3.** Hourly averaged time series of simulated significant wave height ( $H_s$ ) (a), mean wave direction (MWD) (b), and peak wave period ( $T_p$ ) (c) from output of the mesoscale-driven (D03) and LES-driven (D04) domains, compared to wave buoy measurements on the 5th of December.



### 3.2 Evaluation of simulated mean flow

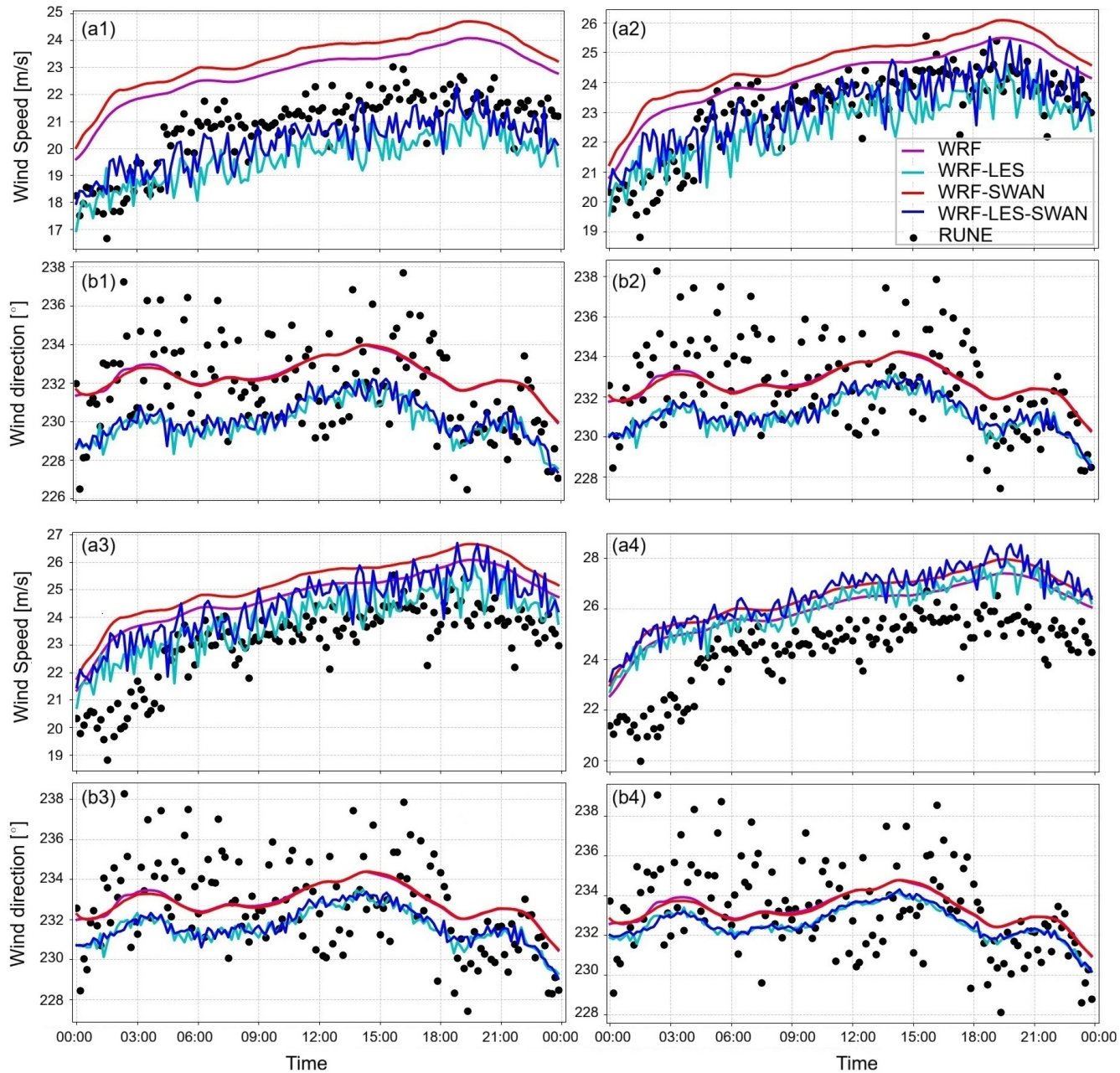
The time series of mean wind speed and direction output from both WRF-SWAN (coupled) and WRF-only (uncoupled) simulations of the mesoscale D03 domain and the LES D04 domain are compared against the lidar measurements at four different heights, 40, 79, 97, and 147 m, in Fig. 4. To ensure temporal consistency with the mesoscale results and measurements, the LES outputs were averaged over 10-min intervals from the 10-s data. At 40 m, the lowest measurement height, simulations from the LES domain (both WRF-LES-SWAN and WRF-LES) show better agreement, in terms of magnitude and variability, with observations than those from the mesoscale domain. At 79 m, the WRF-LES-SWAN simulation exhibits the best agreement with measurements. Above 97 m, WRF-LES-SWAN tends to overestimate the wind speed compared to observations, and above 147 m, the WRF-LES simulation also overestimates the observed wind speed, likely caused by biases in the boundary conditions used to forced the simulations.

which can primarily be attributed to the effect of boundary conditions, as ERA5 overestimates the measurements by up to  $3\text{ ms}^{-1}$  at some time steps.

**Table 2.** The root mean square error (RMSE) computed between observations and simulations. The simulated significant wave height ( $H_s$ ), mean wave direction (MWD), peak period (Tp), wind speed and wind direction are from the D03 and D04 model outputs. WRF and WRF-SWAN are taken from D03 for the uncoupled and coupled simulations, while WRF-LES and WRF-LES-SWAN are taken from D04. The wind speed and direction statistics are calculated for each of the heights from 40 up to 147 m and then averaged.

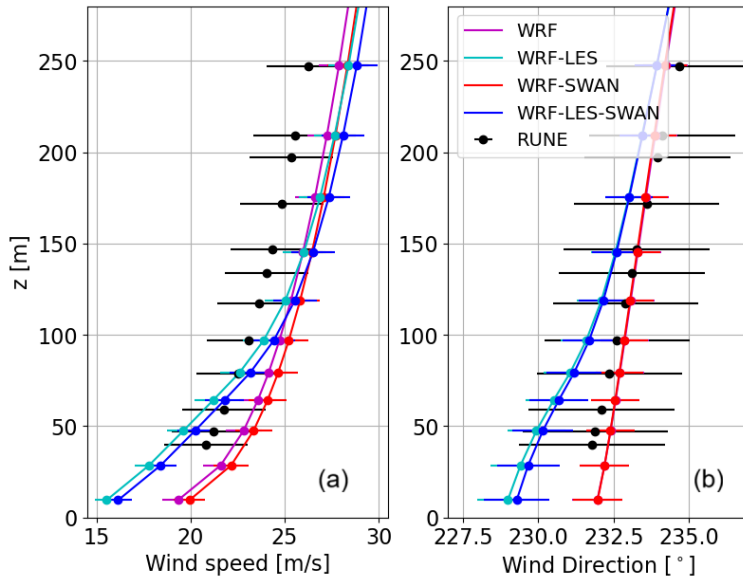
Variable	WRF-SWAN	WRF-LES-SWAN	WRF	WRF-LES
$H_s$ [m]	0.75	<b>0.44</b>	—	—
MWD [°]	<b>6.61</b>	7.02	—	—
Tp [s]	0.97	<b>0.92</b>	—	—
Wind speed [ $\text{m s}^{-1}$ ]	2.71	<b>1.81</b>	2.28	1.87
Wind direction [°]	<b>2.48</b>	3.06	<b>2.48</b>	3.16

Figure 5 presents the vertical profiles of wind speed and direction during the 2-hour period surrounding the time of maximum wave height. Both WRF-LES and WRF-LES-SWAN simulations show lower wind speeds near the surface, which results in close agreement with measurements between 40 and 150 m, as also evident in the RMSE values. However, this is due to excessive vertical wind shear that is attributed to the SGS model used for the LES domain (Peña and Mirocha, 2024). In contrast, WRF and WRF-SWAN show wind profiles with vertical wind shears that are consistent with those from the measurements. In addition, slightly higher wind speeds are observed in the coupled simulations compared to the uncoupled ones. The WBLM, which accounts for wave impacts and calculates an effective roughness length, can yield lower roughness length values than those from the Charnock-based parameterization (Charnock, 1955) used by default in WRF, particularly under stormy conditions. Lower roughness lengths lead to higher surface wind speeds under the same forcing conditions; similar results were reported by Larsén et al. (2019). In terms of wind direction, both WRF-LES and WRF-LES-SWAN simulations show a slight eastward deviation, with a maximum of approximately  $4^\circ$  up to 100 m, which is due to lower



**Figure 4.** Time series of 10-min means of simulated (a\*) wind speed and (b\*) wind direction from the mesoscale (D03) and LES (D04) domains for both coupled (WRF-SWAN) and uncoupled (WRF) simulations, compared to lidar buoy data at a height of (\*1) 40 m, (\*2) 79 m (\*3) 97 m and (\*4) 147 m.

205 simulated  $u$  velocities within the LES simulations, which is linked to the excessive vertical wind shear within LES domains using such a SGS model.



**Figure 5.** Vertical profiles of (a) wind speed and (b) wind direction 7:00 UTC to 19:00 UTC from the D03 and D04, for both coupled and uncoupled simulations, compared with lidar buoy measurements from 17:00 UTC to 19:00 UTC.

### 3.3 Turbulent fluxes

Although no high-frequency measurements are available for in-depth validation, we investigate the behavior of turbulent fluxes of the coupled and uncoupled simulations using results from the LES domains. For this, we compute both the resolved and the 210 SGS stress components. To capture the extreme event at the RUNE measurement location, we use 10-s model outputs over a 2-hour period from 02:00 UTC to 04:00 UTC. The resolved (res) stress components ( $\tau_{ij}^{\text{res}}$ ) for each velocity pair are computed as

$$\tau_{ij}^{\text{res}} = -\rho \langle u'_i u'_j \rangle, \quad (1)$$

where  $\rho$  is the air density,  $u_i$  and  $u_j$  are the along-wind and cross-wind components, the primes ('') denote fluctuations from 215 the mean value, and the angle brackets  $\langle \cdot \rangle$  indicate a temporal average.

The SGS part of the stress includes the deviatoric component  $\tau_{ij}^{\text{dev}}$  and the part from the SGS turbulent kinetic energy  $e_{\text{sgs}}$ . Using the 10-s model outputs (D04 outputs  $e_{\text{sgs}}$  and the deviatoric stresses), the SGS stress is calculated as

$$\tau_{ij}^{\text{sgs}} = \frac{2}{3} \delta_{ij} e_{\text{sgs}} + \tau_{ij}^{\text{dev}}, \quad (2)$$

and the total stress components are obtained from

$$\tau_{ij}^{\text{tot}} = \tau_{ij}^{\text{res}} + \langle \tau_{ij}^{\text{sgs}} \rangle. \quad (3)$$



Figure 6 shows the vertical profiles of the velocity variances  $\langle u'u' \rangle$ ,  $\langle v'v' \rangle$ , and  $\langle w'w' \rangle$ , as well as the covariances  $\langle u'w' \rangle$  and  $\langle v'w' \rangle$ . The Fig. includes both resolved and total (resolved + SGS) fluxes from the WRF-LES and WRF-LES-SWAN simulations at 100 m (D04) and 4 m (D06) horizontal grid spacings. The covariances  $\langle u'w' \rangle$  and  $\langle v'w' \rangle$  exhibit similar trends, with smaller resolved turbulence for D04 compared to D06, as expected from the effect of the spatial resolution difference.

225 Results from both domains clearly show increased turbulence levels when wind–wave interactions are included in the simulation. Similar enhancements in velocity variances were also observed in an idealized simulation of the same case (Hamzeloo et al., 2025). For D04, the turbulence flux (horizontal velocity variances) has its maximum at 70 m, which is rather far from the surface. This is an effect of the coarse horizontal grid spacing of D04 (100 m). When finer horizontal grid spacings of 20 m 230 (D05) and 4 m (D06) are used, the heights of the maximum turbulence fluxes appear closer to the surface, at a height of 60 m and 30 m, respectively. In Hamzeloo et al. (2025), a horizontal grid spacing of 1.25 m was used, and the corresponding height of the maximum turbulence fluxes was confined below the first 5 m. The contribution of SGS stresses is also more evident in D04 compared to D05 (not shown) and D06, as expected. The resolved vertical variances (dashed lines in Fig. 6c) are small in D04, and reach more realistic values (up to  $0.1 \text{ m}^2 \text{ s}^{-2}$ ) in D06.

### 3.4 The impact of cell perturbation method

235 Figure 7 shows the 24-hr time series of wind speed at 40 m from the nested LES domain (D04), with and without CPM. The results highlight the role of CPM in enhancing wind speed variability and fluctuations. To further detail the enhancement of turbulence by using CPM, we compute in Fig. 8 the wind speed spectrum from lidar measurements, the finest mesoscale domain (D03), and the nested LES domain (D04), both with and without CPM. The spectrum is an average of spectra derived within 5 hr windows with a 15-min overlap. As illustrated, the spectrum from the no-CPM case fails to capture the levels 240 of turbulent energy in the measurements even at time scales much larger than 10-min and closely resembles the mesoscale spectrum, which is not expected to resolve turbulence. In contrast, the D04 simulation with CPM activated closely matches the spectral energy distribution of the measurements. The drop of energy at higher frequencies of the spectrum for WRF-LES with CPM can be noticed beyond the timescale of 1-min, which shows the limitation of coarse LES outputs to properly reproduce the range of turbulence scales.

## 245 4 Discussion

With WRF in LES mode successfully coupled with SWAN within the COAWST system, simulations were carried out during a 1-day storm event in the North Sea. Comparison between coupled and uncoupled LES simulations shows that wave–atmosphere interactions have a measurable impact on both mean flow and turbulence characteristics. The improved agreement in the significant wave height and mean wind speed up to 100 m when using the coupled WRF-LES-SWAN model indicates the 250 importance of the online coupling, as their feedback modifies the exchanges in the WBL. This is mainly due to improvements in surface roughness and momentum fluxes estimations, which impact the wind field near the ocean surface. However, the

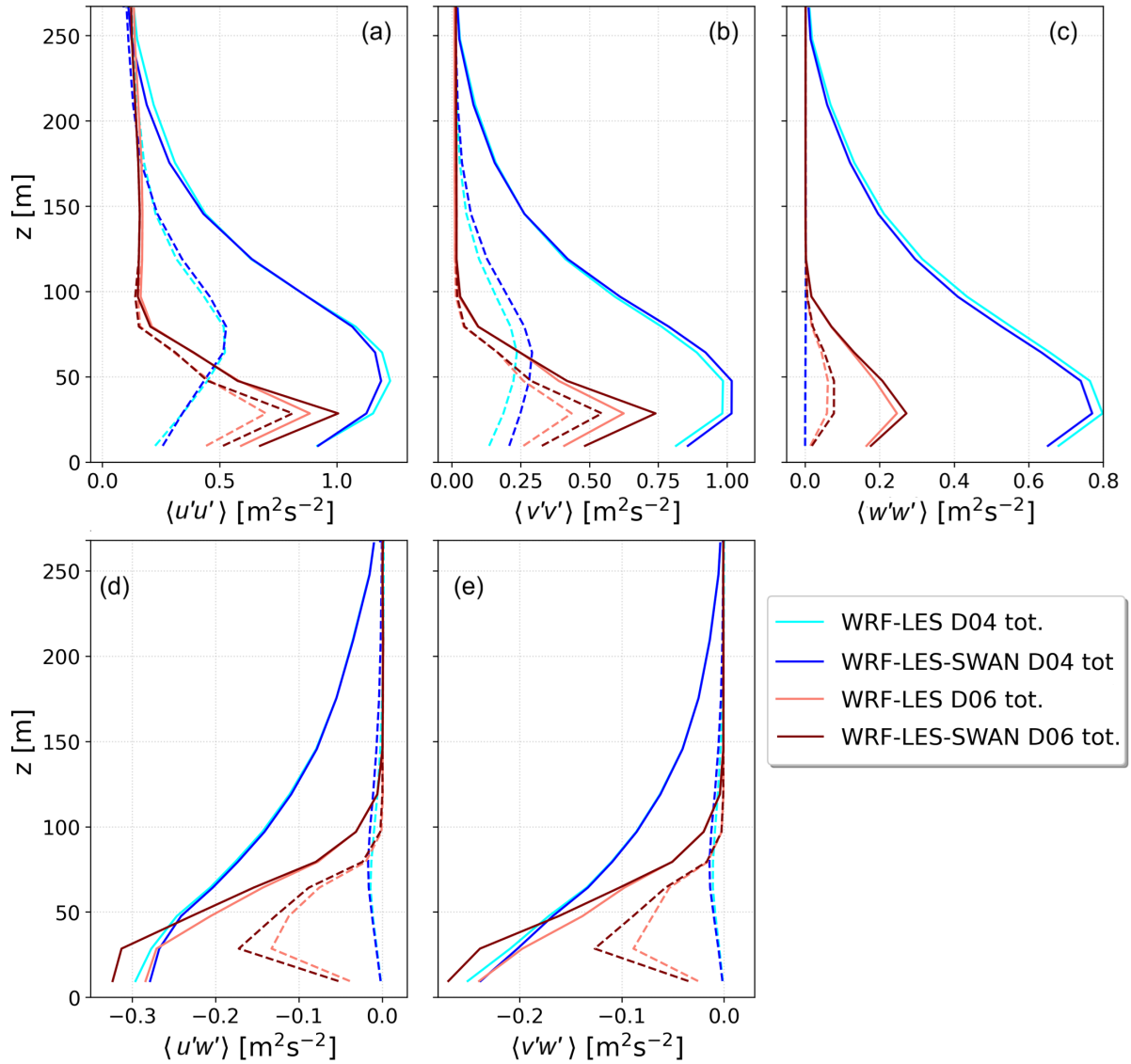


**Figure 6.** Vertical profiles of velocity variances (a)  $\langle u'u' \rangle$ , (b)  $\langle v'v' \rangle$ , (c)  $\langle w'w' \rangle$ , and covariances (d)  $\langle u'w' \rangle$ , (e)  $\langle v'w' \rangle$  and from WRF-LES and WRF-SWAN-LES simulations at 100 m (D04) and 4 m (D06) grid spacings. Dashed and solid lines are representative for resolved and total (resolved + SGS) fluxes.

relatively small differences in mean wave direction and peak wave period show that not all wave parameters are equally sensitive to the coupling, and the benefits may depend on the specific conditions of the event.

The vertical wind profiles indicate that the better statistics on mean winds in Table 2 for the LES type simulations are achieved due to excessive vertical wind shear in LES near the surface caused by the SGS model. In contrast, the mesoscale

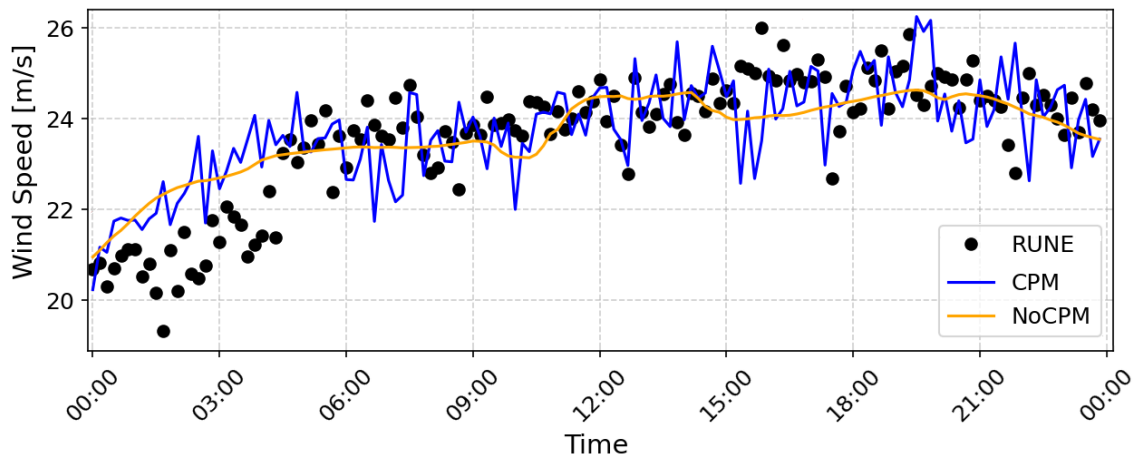


**Figure 7.** 10-min time series of wind speed at 100 m from the D04 simulation, with and without activating the CPM, compared to that from measurements.

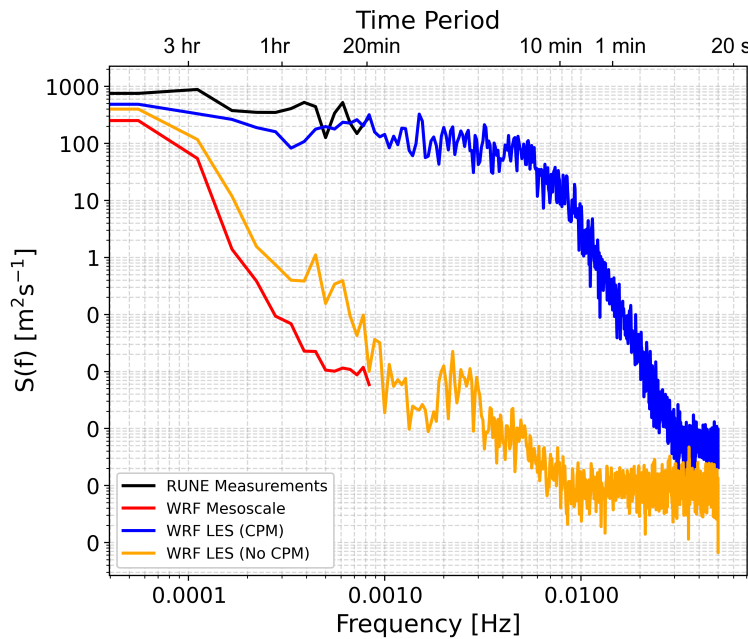


**Figure 8.** Spectrum of wind speed at 100 m from mesoscale domain (D03), and LES domain (D04) with and without CPM compared to that from measurements.

simulations reproduce the vertical wind shear and veer closely with that of the observations, although the LES runs capture greater variability in wind speed. All of the simulations have a bias in the upper atmospheric levels, which might be due to a bias in boundary conditions.



The analysis shows that the coupled simulation produces higher horizontal and vertical velocity variances, which suggests  
260 enhanced turbulent mixing. This finding is consistent with theoretical expectations (Sullivan et al., 2008) and our previous  
modeling efforts (Hamzeloo et al., 2025). Due to the absence of direct turbulence measurements at the RUNE site, we are  
not able to quantify the accuracy of the turbulence simulations. At the beginning of our analysis, we examine the results  
from domain D04 with a horizontal grid spacing of 100 m. In this configuration, the vertical distribution of turbulence fluxes  
show the largest value at 70-m height and unrealistically small vertical velocity variances. For finer horizontal grid spacings,  
265  $\Delta x = 20$  m, the largest turbulence fluxes were present at slightly lower heights. With further refinement,  $\Delta x = 4$  m, the largest  
turbulence fluxes are at a height of around 25 m, and the vertical velocity variance reached more realistic magnitudes. The  
analysis confirms that a high horizontal grid spacing is essential for capturing the turbulence characteristics close to the surface  
and within a significant portion of the MABL. This is in agreement with the results in Sanchez-Gomez et al. (2025), who  
270 performed a multiscale simulation with two nested LES domains around Hurricane Laura, using horizontal grid spacings of  
33.33 m and 11.11 m. They found that the coarsest simulation could not resolve turbulence close to the surface, while the finer  
resolution matched the turbulence statistics of the measurements.

In addition, we evaluate the impact of the CPM on the LES domain boundaries, which is applied for the first time in the WRF  
model through the COAWST framework. In the simulation without CPM, the LES domain cannot sustain turbulence and the  
results are similar to those of the mesoscale domain. More importantly, the ensemble-averaged wind speed spectrum indicates  
275 that the LES without CPM fails capturing the expected turbulence energy levels, even at the time scales larger than those of 3D  
turbulence. In contrast, LES with CPM produces more realistic spectral energy distributions within a broader range of scales,  
consistent with previous real-time simulation studies (Peña and Mirocha, 2024).

## 5 Conclusions

In this study, we coupled the WRF-LES model with the SWAN model within the framework of COAWST. We applied the  
280 coupled, multiscale, modeling system to a real storm case, and evaluated the model performance in capturing mean wind and  
turbulence characteristics within the MABL.

Both coupled and uncoupled LES results showed better agreement with observations at the heights closer to the surface due  
to excessive vertical wind shear reproduced within the LES domain. Compared to the standalone WRF or WRF-LES simulations,  
285 coupling does not show significant differences in the mean wind speed for this storm case, while improves turbulence  
representation. Turbulence in the layers close to the surface has been shown to be very sensitive to horizontal grid spacing. This  
study also shows that turbulence instigation (through CPM) is essential for reproducing realistic turbulence in LES domains.

For future work, we plan to perform multiscale simulations at a site where high-frequency turbulence measurements are  
available for in-depth analysis of turbulence characteristics. This will allow direct validation of simulated turbulence fluxes and  
help quantify the strengths and limitations of coupled WRF-LES-SWAN configurations under different wind-wave conditions.



290 **Appendix A: Abbreviations**

**CCI** Climate Change Initiative

**COAWST** Coupled Ocean Atmosphere Wave Sediment Transport

**CORINE** Coordination of Information on the Environment

**CPM** Cell Perturbation Method

295 **DHI** Danish Hydraulic Institute

**DTM** Digital Terrain Model

**DTU** Technical University of Denmark

**ECMWF** European Centre for Medium-Range Weather Forecasts

**EMODnet** European Marine Observation and Data Network

300 **ERA5** ECMWF Fifth-Generation Atmospheric Reanalysis

**ESA** European Space Agency

**$H_{max}$**  Maximum wave height

**$H_s$**  Significant wave height

**JONSWAP** Joint North Sea Wave Project

305 **LES** Large-Eddy Simulation

**LiDAR** Light Detection and Ranging

**MABL** Marine Atmospheric Boundary Layer

**MIKE 3 Wave FM** MIKE 3 Wave Flexible Mesh

**MWD** Mean Wave Direction

310 **MYJ** Mellor–Yamada–Janjic

**MYNN** Mellor–Yamada–Nakanishi–Niino

**OSTIA** Operational Sea Surface Temperature and Sea Ice Analysis

**PALM** Parallelized Large-Eddy Simulation Model



**PBL** Planetary Boundary Layer

315 **QNSE** Quasi-Normal Scale Elimination

**RMSE** Root Mean Square Error

**ROMS** Regional Ocean Modeling System

**RRTM** Rapid Radiative Transfer Model

**RUNE** Reducing the Uncertainty of Nearshore Energy

320 **SGS** Subgrid-Scale

**SWAN** Simulating WAves Nearshore

$T_{02}$  Average zero-crossing period

**TKE** Turbulent Kinetic Energy

$T_p$  Peak wave period

325 **UTC** Coordinated Universal Time

**WAM** Wave Model

**WBL** Wave Boundary Layer

**WBLM** Wave Boundary Layer Model

**WRF** Weather Research and Forecasting

330 **WSM6** WRF Single-Moment 6-class microphysics scheme

**YSU** Yonsei University

*Author contributions.* SH implemented the changes in WRF and carried out the simulations and analysis. JF contributed to the understanding of the COAWST workflow, and OGS provided inputs on WRF-LES simulations. XGL, AP, and JF provided supervision and guidance throughout the work. SH wrote the initial manuscript draft. All authors reviewed and commented on the manuscript.

335 *Competing interests.* AP is a member of the editorial board of Wind Energy Science.



*Acknowledgements.* This work is funded by the Independent Research Fund Denmark (Danmarks Frie Forskningsfond DFF) through the ‘multiscale Atmospheric Modeling Above the Seas (MAMAS)’ project (nr. 0217-00055B). SH, XGL and JF acknowledge support from the Horizon Europe project DTWO (J. nr. 101146689). The authors also thank Marc Imberger and Jianting Du for their assistance regarding the COAWST system.



## 340 References

- Alimohammadi, M., Malakooti, H., and Rahbani, M.: Comparison of momentum roughness lengths of the WRF-SWAN online coupling and WRF model in simulation of tropical cyclone Gonu, *Ocean Dynamics*, 70, 1531–1545, <https://doi.org/10.1007/s10236-020-01417-w>, 2020.
- Bolaños, R. and Rørbæk, K.: RUNE, Metocean buoy deployment, Tech. rep., DHI, 2016.
- 345 Bontemps, S., Defourny, P., Radoux, J., Van Bogaert, E., Lamarche, C., Achard, F., Mayaux, P., Boettcher, M., Brockmann, C., Kirches, G., et al.: Consistent global land cover maps for climate modelling communities: current achievements of the ESA's land cover CCI, in: *Proceedings of the ESA living planet symposium*, Edinburgh, vol. 13, pp. 9–13, 2013.
- Booij, N., Holthuijsen, L., and Ris, R.: The SWAN Wave Model for Shallow Water, pp. 668–676, American Society of Civil Engineers, <https://doi.org/10.1061/9780784402429.053>, 1997.
- 350 C3S: ERA5: Fifth generation of ECMWF atmospheric reanalyses of the global climate, <https://cds.climate.copernicus.eu/cdsapp#!/home>, accessed: [date of access], 2017.
- Cambazoglu, M. K., Armstrong, B. N., and Wiggert, J. D.: Development of a daily coastal ocean model for Mississippi Sound and Bight, *Ocean Dynamics*, 74, 987–1004, <https://doi.org/10.1007/s10236-024-01645-4>, 2024.
- Charnock, H.: Wind stress on a water surface, *Quarterly Journal of the Royal Meteorological Society*, 81, 639–640, <https://doi.org/10.1002/qj.49708135027>, 1955.
- 355 Chen, W., Chen, J., Shi, J., Zhang, S., Zhang, W., Xia, J., Wang, H., Yi, Z., Wu, Z., and Zhang, Z.: Impact of a New Wave Mixing Scheme on Ocean Dynamics in Typhoon Conditions: A Case Study of Typhoon In-Fa (2021), *Remote Sensing*, 16, 2024.
- Deardorff, J. W.: Stratocumulus-capped mixed layers derived from a three-dimensional model, *Boundary-Layer Meteorology*, 18, 495–527, 1980.
- 360 DHI: MIKE 3 Wave FM: Scientific Documentation, DHI Group, [https://manuals.mikepoweredbydhi.help/2019/Coast\\_and\\_Sea/MIKE\\_3\\_Wave\\_FM\\_Scientific\\_Doc.pdf](https://manuals.mikepoweredbydhi.help/2019/Coast_and_Sea/MIKE_3_Wave_FM_Scientific_Doc.pdf), 2024.
- Donlon, C. J., Martin, M., Stark, J., Roberts-Jones, J., Fiedler, E., and Wimmer, W.: The Operational Sea Surface Temperature and Sea Ice Analysis (OSTIA) system, *Remote Sensing of Environment*, 116, 140–158, <https://doi.org/10.1016/j.rse.2010.10.017>, advanced Along Track Scanning Radiometer(AATSR) Special Issue, 2012.
- 365 Du, J.: Coupling atmospheric and ocean wave models for storm simulation, Ph.D. thesis, Technical University of Denmark (DTU), DTU Wind Energy, 2017.
- Du, J., Bolaños, R., Larsén, X., and Kelly, M.: Wave boundary layer model in SWAN revisited, *Ocean Science*, 15, 361–377, 2019.
- Du, J., Larsén, X. G., Chen, S., Bolaños, R., Badger, M., and Yang, Y.: The impact of wind–wave coupling with WBLM on coastal storm simulations, *Ocean Modelling*, 180, 102 135, <https://doi.org/10.1016/j.ocemod.2022.102135>, 2022.
- 370 Dudhia, J.: Numerical Study of Convection Observed during the Winter Monsoon Experiment Using a Mesoscale Two-Dimensional Model, *Journal of Atmospheric Sciences*, 46, 3077 – 3107, [https://doi.org/10.1175/1520-0469\(1989\)046<3077:NSOCOD>2.0.CO;2](https://doi.org/10.1175/1520-0469(1989)046<3077:NSOCOD>2.0.CO;2), 1989.
- Feranec, J.: Project CORINE land cover, in: *European Landscape Dynamics*, pp. 39–44, CRC Press, 2016.
- Fischereit, J., Larsén, X., and Hahmann, A.: Climatic Impacts of Wind-Wave-Wake Interactions in Offshore Wind Farms, *Frontiers in Energy Research*, 10, 2022.
- 375 Floors, R., Peña, A., Lea, G., Vasiljević, N., Simon, E., and Courtney, M.: The RUNE Experiment—A Database of Remote-Sensing Observations of Near-Shore Winds, *Remote Sensing*, 8, 884, 2016.



- Hamzeloo, S., Larsén, X., Peña, A., Kistne, S., and Soerensen, J.: The RUNE Experiment—A Database of Remote-Sensing Observations of Near-Shore Winds, Submitted to boundary layer meteorology, 2025.
- Hong, S.-Y., Dudhia, J., and Chen, S.-H.: A Revised Approach to Ice Microphysical Processes for the Bulk Parameterization of Clouds and 380 Precipitation, Monthly Weather Review, 132, 103 – 120, [https://doi.org/10.1175/1520-0493\(2004\)132<0103:ARATIM>2.0.CO;2](https://doi.org/10.1175/1520-0493(2004)132<0103:ARATIM>2.0.CO;2), 2004.
- Hong, S.-Y., Noh, Y., and Dudhia, J.: A New Vertical Diffusion Package with an Explicit Treatment of Entrainment Processes, Monthly Weather Review, 134, 2318 – 2341, <https://doi.org/10.1175/MWR3199.1>, 2006.
- Janjic, Z. I.: The Mellor–Yamada Level 2.5 turbulence closure scheme in the NCEP Eta Model, Office Note, National Centers for Environmental Prediction, 437, 2002.
- 385 Jenkins, A. D., Makin, V., and Kukulka, T.: Modelling the impact of waves on offshore wind turbines, Ocean Dynamics, 62, 941–952, <https://doi.org/10.1007/s10236-012-0532-7>, 2012.
- Jiang, Z., Tang, J., Wang, S., Dong, G., and Wang, S.: Simulation of summer climate over East China by convection-permitting regional air-sea coupled model, Climate Dynamics, 63, 106, <https://doi.org/10.1007/s00382-025-07589-9>, 2025.
- Kain, J. S. and Fritsch, J. M.: Convective Parameterization for Mesoscale Models: The Kain-Fritsch Scheme, pp. 165–170, American Meteorological Society, Boston, MA, ISBN 978-1-935704-13-3, [https://doi.org/10.1007/978-1-935704-13-3\\_16](https://doi.org/10.1007/978-1-935704-13-3_16), 1993.
- 390 Kalvig, S., Reuder, J., and Byrkjedal, Ø.: Wave influenced wind and the effect on offshore wind turbine performance, in: European Wind Energy Association Conference, [https://www.researchgate.net/publication/270282509\\_Wave\\_Influenced\\_Wind\\_and\\_the\\_Effect\\_on\\_Offshore\\_Wind\\_Turbine\\_Performance](https://www.researchgate.net/publication/270282509_Wave_Influenced_Wind_and_the_Effect_on_Offshore_Wind_Turbine_Performance), 2014.
- Larsén, X., Fischereit, J., Hamzeloo, S., Bärfuss, K., and Lampert, A.: Investigation of wind farm impacts on surface waves using coupled 395 numerical simulations, Renewable Energy, 237, 2024.
- Larsén, X. G., Du, J., Bolaños, R., Imberger, M., Kelly, M. C., Badger, M., and Larsen, S.: Estimation of offshore extreme wind from wind-wave coupled modeling, Wind Energy, 22, 1043–1057, [https://doi.org/https://doi.org/10.1002/we.2339](https://doi.org/10.1002/we.2339), 2019.
- Mlawer, E. J., Taubman, S. J., Brown, P. D., Iacono, M. J., and Clough, S. A.: Radiative transfer for inhomogeneous atmospheres: 400 RRTM, a validated correlated-k model for the longwave, Journal of Geophysical Research: Atmospheres, 102, 16 663–16 682, <https://doi.org/10.1029/97JD00237>, 1997.
- Muñoz-Esparza, D. and Kosović, B.: Generation of inflow turbulence in large-eddy simulations of nonneutral atmospheric boundary layers with the cell perturbation method, Monthly Weather Review, 146, 1889–1909, <https://doi.org/10.1175/MWR-D-18-0077.1>, 2018.
- Muñoz-Esparza, D., Kosović, B., Mirocha, J., and van Beeck, J.: Bridging the Transition from Mesoscale to Microscale Turbulence in 405 Numerical Weather Prediction Models, Boundary-Layer Meteorology, 153, 409–440, <https://doi.org/10.1007/s10546-014-9956-9>, 2014.
- Muñoz-Esparza, D., Kosović, B., van Beeck, J., and Mirocha, J.: A stochastic perturbation method to generate inflow turbulence in large-eddy simulation models: Application to neutrally stratified atmospheric boundary layers, Physics of Fluids, 27, 035 102, <https://doi.org/10.1063/1.4913572>, 2015.
- Muñoz-Esparza, D., Lundquist, J. K., Sauer, J. A., Kosović, B., and Linn, R. R.: Coupled mesoscale-LES modeling of a diurnal cycle during the CWEX-13 field campaign: From weather to boundary-layer eddies, Journal of Advances in Modeling Earth Systems, 9, 1572–1594, 410 <https://doi.org/10.1002/2017MS000948>, 2017.
- Nakanishi, M. and Niino, H.: An improved Mellor–Yamada level-3 model: Its numerical stability and application to a regional prediction of advection fog, Boundary-Layer Meteorology, 119, 397–407, 2006.



- Ning, X., Paskyabi, M. B., Bui, H. H., and Penchah, M. M.: Evaluation of sea surface roughness parameterization in meso-to-micro scale simulation of the offshore wind field, *Journal of Wind Engineering and Industrial Aerodynamics*, 242, 105 592, 415  
https://doi.org/https://doi.org/10.1016/j.jweia.2023.105592, 2023.
- Olabarrieta, M., Warner, J., Armstrong, B., Zambon, J., and He, R.: Ocean-atmosphere dynamics during Hurricane Ida and Nor'Ida: An 420 application of the coupled ocean-atmosphere-wave-sediment transport (COAWST) modeling system, *Ocean Modelling*, 43-44, 112–137, 2012.
- Peña, A. and Mirocha, J. D.: One-year-long turbulence measurements and modeling using large-eddy simulation domains in the Weather 425 Research and Forecasting model, *Applied Energy*, 363, 123 069, https://doi.org/https://doi.org/10.1016/j.apenergy.2024.123069, 2024.
- Porchetta, C., Sullivan, P. P., and McWilliams, J. C.: Wind–wave interactions and their impact on the marine atmospheric boundary layer in 430 offshore wind energy applications, *Frontiers in Energy Research*, 10, 881 459, https://doi.org/10.3389/fenrg.2022.881459, 2022.
- Sanchez-Gomez, M., Deskos, G., and Lundquist, J. K.: Turbulence-resolving simulations of Hurricane Laura (2020): Insights into extreme 425 winds and eyewall turbulence, *Quarterly Journal of the Royal Meteorological Society*, https://doi.org/10.1002/qj.70003, first published: 29 August 2025, 2025.
- Shaw, W. J., Berg, L. K., Debnath, M., Deskos, G., Draxl, C., Ghate, V. P., Hasager, C. B., Kotamarthi, R., Mirocha, J. D., Muradyan, P., 430 Pringle, W. J., Turner, D. D., and Wilczak, J. M.: Scientific challenges to characterizing the wind resource in the marine atmospheric boundary layer, *Wind Energy Science*, 7, 2307–2334, https://doi.org/10.5194/wes-7-2307-2022, 2022.
- Skamarock, W., Klemp, J., Dudhia, J., Gill, D., Liu, Z., Berner, J., and Huang, X.-y.: A description of the advanced research WRF model 435 version 4.1, 2019.
- Sukoriansky, S., Galperin, B., and Perov, V.: A quasi-normal scale elimination model of turbulent flows with stable stratification, *Physics of Fluids*, 17, 085 107, 2005.
- Sullivan, P. P., McWilliams, J. C., and Moeng, C.-H.: LES of Marine Atmospheric Boundary Layers over a Wavy Surface, *Journal of the 440 Atmospheric Sciences*, 65, 1225–1245, 2008.
- Tewari, M., Chen, F., Wang, W., Dudhia, J., LeMone, M. A., Mitchell, K., Ek, M., Gayno, G., Wegiel, J., and Cuenca, R. H.: Implementation 445 and verification of the unified Noah land surface model in the WRF model, in: 20th Conference on Weather Analysis and Forecasting/16th Conference on Numerical Weather Prediction, American Meteorological Society, https://opensky.ucar.edu/islandora/object/conference%3A1576, 2004.
- Warner, J., Armstrong, B., He, R., and Zambon, J.: Development of a Coupled Ocean–Atmosphere–Wave–Sediment Transport Modeling 440 System, *Ocean Modelling*, 35, 230–244, 2010.
- Yang, X., Shen, L., and Sotiropoulos, F.: Large-eddy simulations of wind–wave–turbine interactions over the ocean, *Journal of Fluid Mechanics*, 755, R1, https://doi.org/10.1017/jfm.2014.396, 2014.